

Towards a Precision Measurement of Binary Black Holes Formation Channels Using Gravitational Waves and Emission Lines

Suvodip Mukherjee^{1,*} and Azadeh Moradinezhad Dizgah^{2,†}

¹*Perimeter Institute for Theoretical Physics, 31 Caroline Street N., Waterloo, Ontario, N2L 2Y5, Canada*

²*Département de Physique Théorique, Université de Genève,
24 quai Ernest Ansermet, 1211 Genève 4, Switzerland*

(Dated: November 29, 2021)

The formation of compact objects—neutron stars, black holes, and supermassive black holes—and its connection to the chemical composition of the galaxies is one of the central questions in astrophysics. We propose a novel *data-driven*, multi-messenger technique to address this question by exploiting the inevitable correlation between gravitational waves and atomic/molecular emission line signals. We show that the minimum delay time of 0.5 Gyr and the power-law index $\kappa = 1$ of the fiducial scenario of the probability distribution function $p(t_d) \propto t_d^{-\kappa}$ is possible with a standard deviation 0.12 (and 0.45) and 0.06 (and 0.34) respectively from five years of LIGO-Virgo-KAGRA observation in synergy with SPHEREx line intensity mapping (and DESI emission-line galaxies).

Introduction – Gravitational waves discovered by the LIGO-Virgo-KAGRA (LVK) scientific collaboration [1–7] has opened a new window to explore the cosmos using coalescing compact objects such as binary neutron stars (BNS), binary black holes (BBH), and neutron star - black hole (NSBH) systems [8–16]. One of the interesting questions that we can learn about from these measurements is the population of binary compact objects and their merger rate with cosmic time [10, 11, 14, 17]. The merger rate of BBH as a function of redshift, inferred until O3 LVK observation, is in agreement with a power-law form $(1+z)^\gamma$, with $\gamma = 2.7_{-1.7}^{+1.8}$ for $z < 1$ [14].

One of the key questions that the observed population of GW sources can shed light on is how these black holes form in the Universe and how their formation relates to the stellar population through cosmic star formation rate (SFR), stellar mass, and stellar metallicity. The dependence of the binary merger population on these quantities is not yet known from the data. Several simulations have explored the connection between stellar properties and different types of compact objects such as BNS, NSBH, and BBHs [17–20]. However, inference of the connection of GW compact objects with host galaxies from observations is difficult to achieve due to the large sky localization error of the GW sources.

We propose a novel multi-messenger technique to probe this connection by taking advantage of synergies between atomic and molecular emission lines such as H α , H β , [OII], [OIII], [NII], CO, [CII] as tracers of the stellar properties and GW sources such as BNS, NSBH, and BBHs as tracers of compact objects. The spectral lines can be detected either as aggregate signals using the emerging technique of line intensity mapping (LIM) [21] or in individually resolved galaxies by spectroscopic galaxy surveys probing emission-line galaxies (ELGs). The dependencies of the emission lines and GW sources on stellar populations lead to an inevitable correlation between these two sectors. The luminosity of emission

lines determines the amplitude and redshift-dependence of the line power spectrum signal measured by LIM surveys, and the mean number densities of galaxies probed by galaxy surveys. Therefore, the correlation between the observations in GWs and emission lines can provide a model-independent measurement of the dependence of the compact object population on the SFR and stellar mass and metallicity. We illustrate the measurement prospects of this correlation from the currently ongoing network of GW detectors such as LVK in synergy with LIM with upcoming space mission SPHEREx [22], and ELGs detectable by the ongoing DESI galaxy survey [23]. Previous studies have explored the synergy between LVK with SPHEREx and DESI galaxy samples for the cross-correlation studies to measure cosmological parameters, and GW bias parameter [24, 25] and also with Einstein Telescope [26].

Relating GW sources and galaxy properties – Several formation channels for binary compact systems such as BNS, BBH, and NSBH have been proposed in the literature [27–37]. Different channels lead to different delay time distributions $P(t_d)$ which captures the time between the formation of stars and merging of the compact objects. The delay time distribution will leave an imprint on the merger rates of binary systems, their redshift evolution, and their connection with the host galaxies. The merger rate of the binary compact objects can be written in terms of the delay time distribution $P(t_d)$, and the SFR density $R_{\text{SFR}}(z)$ by the relation

$$N_{\text{GW}}(z_m) = \mathcal{N} \int_{z_m}^{\infty} dz \frac{dt_f}{dz} P(t_d) R_{\text{SFR}}(z), \quad (1)$$

where \mathcal{N} is the normalization constant to set the local merger rate of GW sources with the observed value [14–16]. The probability distribution of the delay time distribution is expected to follow a power-law form $P(t_d) = t_d^{-\kappa}$ with the value of $\kappa = 1$ for an initial logarithmic distribution of the separation of the compact objects [38].

However, from simulations, it is shown that the minimum value of delay time and the power-law index of the probability distribution can be different $\kappa \neq 1$ [19, 39]. Recent works [19, 39] based on population synthesis simulations combined with galaxy catalogs from the hydrodynamic simulations have shown that a different delay time distribution of the GW sources can lead to a different dependence of the compact object mergers on the stellar mass (M_*), SFR, and stellar metallicity (Z) of the host galaxy, which can be expressed by the relation [19]

$$\log(n_{\text{GW}}/\text{Gyr}^{-1}) = \gamma_1 \log(M_*/M_\odot) + \gamma_2 \log(Z/Z_\odot) + \gamma_3 \log(\text{SFR}/M_\odot\text{yr}^{-1}) + \gamma_4. \quad (2)$$

However, we do not have a direct measurement confirming this relation from the LVK data. Recent studies from individual events [40] and the stochastic GW background [41] have only been able to put an upper bound on the delay time, assuming a fixed SFR. The measurement of the delay time distribution will be a direct probe to understand the dependence of the binary compact objects on the stellar properties. In Fig. 1, we show the merger rate of the GW sources for two values of the minimum delay time t_d^{min} (in red and blue), assuming two different models of the SFR; Madau-Dickinson [42] (dashed lines) and Behroozi [43] (solid lines). The plot indicates the possible variation in the merger rate evolution with redshift even for the same model of delay time distribution but with a different SFR model. Previous studies [44–46] have explored how to explore the delay time for BNS. In this work, we explore how the delay time distribution can be inferred for BBH.

The dependence of the merger rates of GW sources on SFR and metallicity can be determined in a model-independent way by comparing with the electromagnetic (EM) tracers of the stellar properties. Emission lines from well-resolved galaxies (in galaxy surveys) or the aggregate signal from individually unresolved galaxies (in LIM surveys) provide excellent tracers of these properties. At an individual level, the correlation between a galaxy and GW sources is not measurable due to a large sky localization error of the GW signal [5]. Nevertheless, we can infer the dependence of GW signal on stellar properties by comparing the number density of GW sources with the sky-averaged number density (and intensity) of ELGs or with the strength of the sky-averaged line intensity signal and its redshift dependence in a statistical way. Also, as we are exploring all-sky quantities, we do not need overlapping sky areas of the GW sources and ELGs (or LIM). In this method, as we are not doing cross-correlation of the GW sources with EM probes [25, 26, 47–55], so the results are not susceptible to poor sky localization error of the GW sources. For GW sources with very good sky localization, spatial cross-correlation with EM probes to explore the delay time is also a possibility.

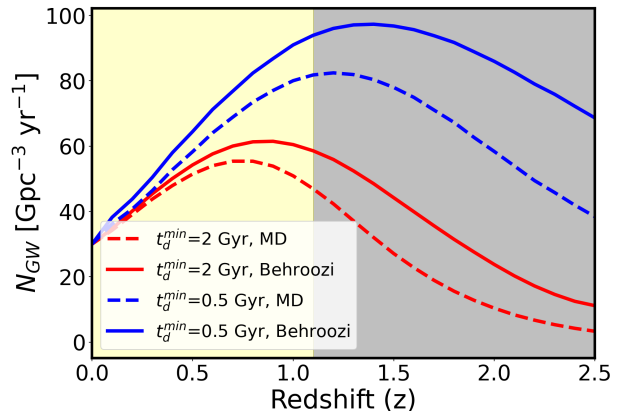


FIG. 1: The merger rate of GW sources for Madau-Dickinson (MD) and Behroozi models of SFR for two different values of the minimum delay time $t_d^{\text{min}} = 0.5$ Gyr and 2 Gyrs. Yellow shaded region denotes the maximum redshift range up to which GW sources can be detected by the LVK detectors. Grey shaded region is accessible by the stochastic GW background.

EM probes of the galaxy properties – In general, the luminosities of the emission lines trace the star formation and are expected to be correlated with astrophysical properties of the galaxies. In analogy with Eq. (2), this relation can be parameterized as

$$\log(L_{\text{line}}/L_\odot) = \alpha_1 \log(M_*/M_\odot) + \alpha_2 \log(Z/Z_\odot) + \alpha_3 \log(\text{SFR}/M_\odot\text{yr}^{-1}) + \alpha_4, \quad (3)$$

where, α_n are the unknown coefficients of the fit, which vary for different lines. For instance, while [OIII], [OII], and [CII] lines are expected to have a strong dependence on metallicity, $\text{H}\alpha$, and $\text{H}\beta$ lines should not [56, 57].

Connecting line luminosities to astrophysical properties of galaxies and SFR at low and high redshifts is an active field of research [56–61]. In the absence of models consistently accounting for such dependencies, line luminosities are often modeled using scaling relations based on fits to the local universe or numerical simulations [62–67]. In this paper, as the first application of our proposed data-driven technique, we use the existing scaling relations used in Ref. [66] to relate L_{line} and SFR, assuming both quantities to depend only on halo mass and redshift, $\text{SFR}(M, z) = \Gamma_{\text{line}} \times L_{\text{line}}(M, z)$, with Γ_{line} being the scaling coefficient for a given line. We use the empirical fit from [43] for $\text{SFR}(M, z)$. To have redshift overlap with LIGO observations ($z \leq 1.1$), we consider rest-frame optical lines $\text{H}\alpha$ 6563Å, [OIII] 5007Å, and [OII] 3727Å probed by SPHEREx LIM. Furthermore, we consider the mean number densities of [OII] ELGs detected by DESI. Based on Ref. [66], taking SFR in unit of [$M_\odot\text{yr}^{-1}$] and luminosity in unit of [erg s^{-1}], we consider the scaling coefficients of $\Gamma_{\text{line}} = (7.9, 7.6, 14) \times 10^{-42}$ for $\text{H}\alpha$, [OIII],

and [OII] lines, respectively.

We compute the mean number density of individually resolved line emitters by matching the minimum mass (M_{\min}) of halos hosting line-luminous galaxies to the minimum luminosity (L_{\min}) detectable by DESI. Therefore, we have $\bar{n}(z) = \int_{M_{\min}}^{M_{\max}} dM n(M, z)$, and using the line luminosity - halo mass relation, we compute the M_{\min} corresponding to $\log_{10}(L_{\min}/\text{erg s}^{-1}) = (40.5, 41)$ for redshift ranges $0.65 \leq z < 1$, and $1 \leq z \leq 1.65$, correspondingly. These values are broadly in agreement with those in Refs. [68, 69].

For LIM signal, we model the power spectrum using the halo-model framework, which relates the statistical properties of line intensity fluctuations to the abundance and clustering of halos hosting line-luminous galaxies. The total signal in the line power spectrum $P_{\text{LIM}}^{\text{tot}}(k, z) = P_{\text{LIM}}^{\text{shot}}(z) + P_{\text{LIM}}^{\text{clust}}(k, z) + P_N$ consists of three contributions namely, the shot noise $P_{\text{LIM}}^{\text{shot}}(z)$ due to the discrete nature of the line emitting galaxies, the clustering term $P_{\text{LIM}}^{\text{clust}}(k, z)$, which traces the underlying dark matter fluctuations, and the instrument noise P_N . In the Poisson limit we have

$$P_{\text{LIM}}^{\text{shot}}(z) = \int_M n(M, z) \left[\frac{L_{\text{line}}(M, z)}{4\pi \mathcal{D}_L^2(z)} \left(\frac{dl}{d\theta} \right)^2 \frac{dl}{d\nu} \right]^2, \quad (4)$$

where $n(M, z)$ is the halo mass function, \mathcal{D}_L is the luminosity distance, and $(dl/d\theta)^2 dl/d\nu$ reflects the conversion from comoving volume to observed specific intensity volume defined in terms frequency, ν , and angular size, θ . We set the limits of mass integration to be $(M_{\min}, M_{\max}) = (10^9, 10^{13}) M_{\odot} h^{-1}$. In the absence of anisotropies, and assuming linear biasing relation between the line intensity and dark matter fluctuations, the clustering component is given by

$$P_{\text{LIM}}^{\text{clust}}(k, z) = \bar{I}_{\text{line}}^2(z) [b_1^{\text{line}}(z)]^2 P_0(k, z), \quad (5)$$

where b_1^{line} is the linear line bias (which is a normalized, mass averaged, and luminosity weighted linear halo bias), P_0 is the linear matter power spectrum, and $\bar{I}_{\text{line}}(z)$ is the mean intensity of the line,

$$\bar{I}_{\text{line}}(z) = \int_M n(M, z) \frac{L_{\text{line}}(M, z)}{4\pi \mathcal{D}_L^2(z)} \left(\frac{dl}{d\theta} \right)^2 \frac{dl}{d\nu}. \quad (6)$$

The observed clustering power of line fluctuations is anisotropic due to redshift-space distortions [70, 71], and the Alcock-Paczynski effect [72]. Furthermore, the power spectrum receives additional contributions due to interloper lines, which fall in the same frequency band as the signal of interest [73–75]. The explicit expressions of the anisotropic clustering power, including line interlopers, which we use in this work, can be found in Refs. [75, 76].

The overall amplitude of LIM signal is represented by the root mean square (RMS) (σ_{ℓ} for $\ell = 0, 2, 4$),

of the three lowest moments of the power spectrum, P_{ℓ} , smoothed on the scale of $R_s = 8 h^{-1} \text{Mpc}$ with a smoothing kernel $W(R_s, k)$. Therefore, $\sigma_{\ell}^2(z) = \Sigma_i k_i^2 \Delta k / (2\pi)^2 W^2(R_s, k_i) P_{\ell}(k_i, z)$, with k_i being the wavenumber in the i^{th} k-bin of width Δk , set to be the fundamental mode of the survey, k_f . The upper bound of the sum is set to $k_{\max} = 0.3 \text{Mpc}^{-1} h$.

Expected correlation between the GW signal and the emission line signal – The relation between the number density of GW sources and global SFR, stellar mass, and metallicity in Eq. (7) can be described in matrix form as ¹

$$\mathbf{N}(z) = \mathbf{G}(z)\mathbf{S}(z), \quad (7)$$

where $\mathbf{N}(z) = [n_{\text{BNS}}(z), n_{\text{NSBH}}(z), n_{\text{BBH}}(z)]$ refers to the number density of GW sources of the three binary types, and \mathbf{G} is a matrix of the coefficients of the relation between the number densities of GW sources and the astrophysical properties of the galaxies, represented by $\mathbf{S}(z)$. Similarly, given the dependence of line luminosity on SFR, stellar mass, and metallicity in Eq. (3), the relation between EM signal and these astrophysical properties can be cast in matrix form as

$$\mathbf{E}(z) = \mathbf{A}(z)\mathbf{S}(z), \quad (8)$$

where $\mathbf{E}(z)$ can be the intensity of the ELGs or RMS fluctuation of the LIM signal for different lines, and \mathbf{A} is a matrix whose coefficients relate the observed strength of the emission line signal with the global astrophysical properties, represented by \mathbf{S} . Since both GW sources and their merger rate and the line emission depend physically on the same astrophysical quantities, we can combine Eqs. (7) and (8) as

$$\mathbf{N}(z) = \mathbf{G}(z)\mathbf{A}^{-1}(z)\mathbf{E}(z) \equiv \mathbf{K}(z)\mathbf{E}(z), \quad (9)$$

where, $\mathbf{K}(z) \equiv \mathbf{G}(z)\mathbf{A}^{-1}(z)$ denotes the matrix whose coefficients capture the connection between the GW source properties and the emission line signal. In the above equation, $\mathbf{N}(z)$ and $\mathbf{E}(z)$ can be measured from GW and EM observations, respectively. Although the connection matrices \mathbf{G} and \mathbf{A} are not well known, we can infer the matrix \mathbf{K} by combining the two independent observations, without invoking any model. The redshift uncertainties in the measurements of $\mathbf{N}(z)$ and $\mathbf{E}(z)$ set the accuracy with which the redshift-dependence of $\mathbf{K}(z)$, which carries information about the formation channels of the binary compact objects, can be determined. The redshift uncertainty of the EM measurement and the luminosity distance uncertainty in the GW signal can be incorporated in the above equation with a window function, $\mathbf{W}(z, z')$ and $\mathbf{D}(\mathcal{D}_L, z)$, which modifies Eq. (9) to

$$\mathbf{N}(z) \equiv \mathbf{D}(\mathcal{D}_L, z)\mathbf{N}(\mathcal{D}_L) = \mathbf{K}(z)\mathbf{W}(z, z')\mathbf{E}(z'). \quad (10)$$

¹ Bold fonts denote matrices.

In Fig. 2, we show the correlation between the GW sources and the emission line signal, assuming SFR of Behroozi, and a delay time distribution of the form $P(t_d) \propto t_d^{-\kappa}$ with two different values of the minimum delay time parameter of $t_d^{\min} = 0.5$ Gyr and 2 Gyr (shown in small- and large-size markers, respectively). The top panel shows the correlation between N_{GW} with the RMS fluctuation of the LIM signal, while the bottom panel shows the correlation with the mean intensity of ELGs. The three curves from top to bottom in each panel, shown by circles, crosses, and stars, correspond to $\text{H}\alpha$, $[\text{OIII}]$, and $[\text{OII}]$ lines. This plot indicates that the trajectory of the correlation between emission lines and GW shows different behavior for different delay time scenarios. If the delay time is small, then the GW sources will exhibit a longer correlation with the emission line signals before turnover, in comparison to the case of a large delay time. Moreover, depending on whether the strength of the emission lines signals strongly correlates at all redshifts, the correlation will show a positive helicity, in comparison to a negative helicity when the GW sources will not follow the emission lines signal up to a high redshift.

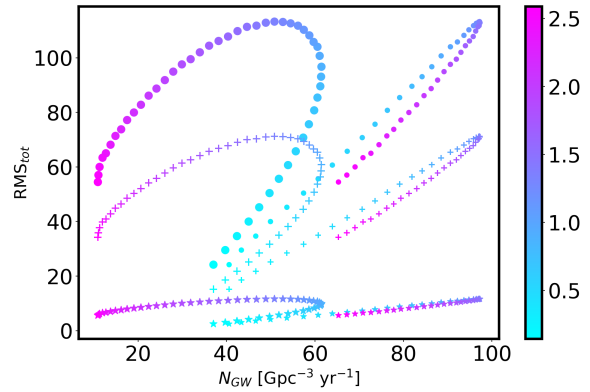
It is noteworthy that GW sources of different masses can exhibit slightly different dependence on the delay time, hence a different dependence on the emission line. The probability distribution $P(t_d, \mathcal{M}) = t_d^{-\kappa(\mathcal{M})}$ with a value of minimum delay time can have a mass dependence $t_d^{\min}(\mathcal{M})$. Therefore, the mass dependence of the delay time can also be captured using the method presented.

Fisher Forecasts – In this analysis, we only focus on BBH sources detectable in cosmological distances from the near-term GW detectors such as LIGO [1, 2], Virgo [3, 4], and KAGRA [5–7] and what we can learn in synergy with the near-term LIM surveys such as SPHEREx [22] and ELGs from DESI [23]. In future work, we will show how this method will be useful for the CE [77] and ET [78] to understand the formation channel of BNS, NSBH, and for SMBHs from LISA[79], and investigate the potential of other spectral emission lines.

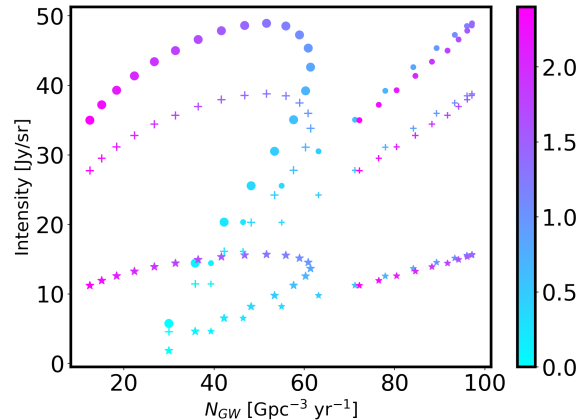
We can write the Fisher information matrix in terms of the parameters $\theta \in \{t_d^{\min}, \kappa\}$ as

$$F_{\alpha\beta} = \frac{1}{2} \sum_{L_i} \sum_{z_k} \sum_{\mathcal{M}_*} \left[\frac{D_{\theta_\alpha} D_{\theta_\beta}}{C(z_k, \mathcal{M}_*, L_i)} + \frac{D_{\theta_\beta} D_{\theta_\alpha}}{C(z_k, \mathcal{M}_*, L_i)} \right], \quad (11)$$

where the first summation is over different lines, the second summation is over the redshift z_k , and the third summation is over different mass-bins of the chirp mass of the GW sources \mathcal{M}_* . The terms $D_{\theta_i} \equiv \partial N_{\text{GW}}(z_k, \mathcal{M}_*) / \partial \theta_i$ and $C(z_k, \mathcal{M}_*, L_i) = \sigma_p^2 + \sigma_e^2 + \sigma_r^2$ denote the covariance matrix, which we consider diagonal and consider three parts to it, namely $\sigma_p^2 = N_{\text{GW}}$ which is the Poisson error on the GW source number, $\sigma_e^2 = (\partial N_{\text{GW}} / \partial L_i)^2 \sigma_{L_i}^2$ is the error in the GW numbers due to change in the luminosity of the i^{th} emission line, and $\sigma_r^2 = (\partial N_{\text{GW}} / \partial z)^2 [(\partial z / \partial \mathcal{D}_L)^2 |_{\Theta_c} \sigma_{\mathcal{D}_L}^2 + \sigma_z^2]$ is the error



(a) Correlation between LIM signal and GW sources.



(b) Correlation between ELGs intensity and GW sources.

FIG. 2: The correlation between the RMS signal of LIM and ELG intensity for $\text{H}\alpha$ (in circle), $[\text{OIII}]$ (in cross), and $[\text{OII}]$ (in star) and GW sources N_{GW} is shown for two different delay time distribution with $t_d^{\min} = 0.5$ Gyr (small marker) and 2 Gyr (large marker) as a function of cosmological redshift (shown by color bar).

in the redshift due to the error in the luminosity distance measurement $\sigma_{\mathcal{D}_L}^2$ for a fixed cosmological parameters denoted by Θ_c (set to Planck-2018 [80] values), and σ_z^2 is the redshift uncertainty in the EM sector. For LIM surveys, the redshift uncertainty $\sigma_z = (1+z)/\mathcal{R}$ is determined by the resolution of the instrument denoted by $\mathcal{R} \equiv \nu/\Delta\nu$ and $\sigma_z = 0.001(1+z)$ for DESI.

The major sources of uncertainty are from the luminosity distance and the Poisson error on the GW sources. The additional uncertainty due to the stochasticity of the delay time distribution specific to the sources is subdominant due to the all-sky averaging of the LIM signal and a large number of ELGs. The standard deviation (Cramer-Rao bound) on a parameter θ_α denoted by Σ_α can be obtained by taking the square-root of the α component of the inverse of the Fisher matrix $\Sigma_\alpha = \sqrt{(\mathbf{F}^{-1})_{\alpha\alpha}}$.

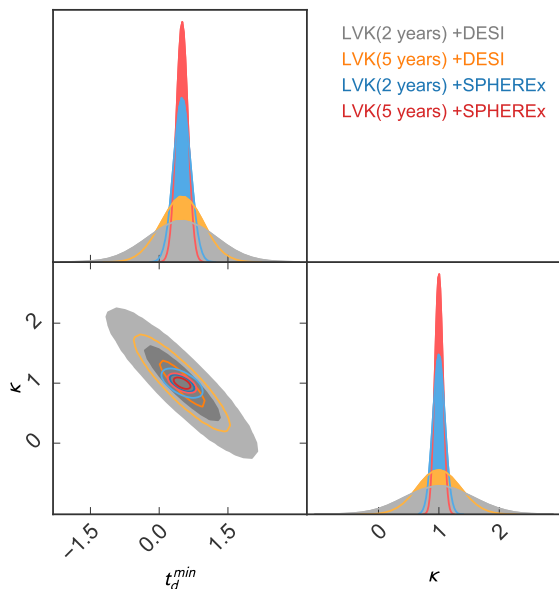


FIG. 3: Fisher forecast for measuring the minimum delay time $t_d^{\min} = 0.5$ Gyr and power-law index κ of the probability distribution $P(t_d) = t_d^{-\kappa}$ using LVK and the emission lines signal from LIM by combining $H\alpha$, [OIII], and [OII] lines from SPHEREx (blue and red), and [OII] ELGs from DESI (grey and yellow).

We consider a population of BBH sources with a power-law mass distribution ($m^{-2.35}$) for the heavier object and m^{-1} for the lighter one. We estimate the matched filtering signal to noise ratio (SNR), ρ , for a binary systems with detector-frame chirp mass \mathcal{M}_d at the luminosity distance of \mathcal{D}_L , using the relation [81, 82]

$$\rho = \rho_* \Theta \left(\frac{\mathcal{M}}{\mathcal{M}_d^*} \right)^{5/6} \left(\frac{\mathcal{D}_L^*}{\mathcal{D}_L} \right), \quad (12)$$

where Θ is the detector projection factor assumed to be uniform between $[0, 1]$. The value of $\rho_* = 8$ is set for the parameters \mathcal{M}_d^* and \mathcal{D}_L^* according to Ref. [5] for the LVK design sensitivity. The combined matched filtering SNR for the network of detectors is obtained by using $\rho_{\text{det}}^2 = \sum_i \rho_i^2$, and we select samples with $\rho_{\text{det}} \geq 10$. We draw posterior samples on the GW source parameters by using the approximate form of the likelihood for the chirp mass and mass-ratio given by [81, 82]. We estimate the posterior distribution on the luminosity distance using a Gaussian approximation. Though the results from individual events are likely to be non-Gaussian, the results after combining several events are not going to vary significantly due to the approximation of the Gaussian posterior by the central limit theorem. So, the Fisher forecast presented in this paper will not be affected by this assumption. The detection of the GW sources of lighter mass sources situated at higher luminosity distances with $\rho_{\text{det}} \geq 10$ is rare. As a result, an appropriate selection function depending on the source properties

also needs to be taken into account. For LIM, we consider the redshift range of $z_{\text{max}} = 1.1$ and $z_{\text{min}} = \{0.2, 0.5, 1.0\}$ for $H\alpha$, [OIII], and [OII] lines, which can be probed in the lowest frequency band of SPHEREx with the spectral resolution of $\mathcal{R} = 41$, and over two 100 deg^2 fields [22, 83]. The instrument noise $P_N(z) = V_{\text{vox}} \sigma_{I, \text{vox}}^2$ depends on the voxel comoving volume V_{vox} and the voxel intensity noise $\sigma_{I, \text{vox}}$. Furthermore, we account for the attenuation of signal due to Fourier spectral and angular point-spread functions, which render the instrument noise scale-dependent (see Ref. [83] for further details). We account for the contamination from both foreground and background line interlopers as outlined in [76]. For DESI, we consider the mean number density of the [OII] emitters at $0.65 \leq z \leq 1.1$ [23].

In Fig. 3, we show the 2D marginalized constraints on the parameters $t_d^{\min} = 0.5$ Gyr and $\kappa = 1$ from a combination of GWs and LIM from SPHEREx and mean number densities of ELGs from DESI using the Fisher formalism. The plots indicate that we can measure delay time parameter and the fiducial model of the power-law index of the probability distribution function with corresponding error-bars of $\Sigma_{t_d^{\min}} = 0.12$ (and 0.18) and $\Sigma_{\kappa} \sim 0.06$ (and 0.095) for 5 years (and 2 years) of observation from LVK in synergy with SPHEREx. Using DESI, the precision on the parameters degrades by about a factor of 3.5 due to the limited availability of ELGs at lower redshift, and also for having only [OII] emission line signal. This shows that a first precise measurement of the delay time distribution will be possible in the near future from LVK.

Conclusions and future prospects – We proposed a novel multi-messenger avenue to explore the formation channel of compact objects by studying the correlation between different emission line signals from ELGs or LIM. We showed that the network of LVK detectors, in conjunction with LIM signal of $H\alpha$, [OIII] lines measured by SPHEREx or number count of ELGs detectable by DESI, can constrain the minimum delay time value and the power-law index of the probability distribution with decent precision. The proposed method can equally be applied to understand the dependence of the compact objects on SFR and metallicity, not only for the stellar-mass black holes, but also for the BNS, NSBH, and also for SMBHs. The connection between BNS, NSBHs, and SMBHs will be possible to explore from the next generation GW detectors such as CE, ET, and LISA in synergy with the multi-line LIM signal and ELGs.

This is the first work showing the potential of this multi-messenger technique to probe the delay time distribution of BBHs. There are several directions in which this technique can be extended. This technique can further shed light on the formation channel of BBHs and can also distinguish primordial black holes (PBHs) populations [41, 84–101]. Future work will explore the feasibility of distinguishing astrophysical BHs from PBHs by this technique. Moreover, in this current work, we have

assumed a fixed value of the cosmological parameters to relate the observed GW sources with emission lines. Joint estimation of the cosmological parameters and the delay time parameter is also possible by this technique. In summary, the combined study of the emission lines and GW sources can play a crucial role in exploring several new territories in astrophysics and fundamental physics.

Acknowledgements – The authors are thankful to Maya Fishbach for reviewing this manuscript and providing useful inputs. The authors would like to thank Olivier Doré, Garrett K. Keating, and Pascal Oesch for valuable inputs. S.M. is supported by the Simons Foundation. Research at Perimeter Institute is supported in part by the Government of Canada through the Department of Innovation, Science and Economic Development and by the Province of Ontario through the Ministry of Colleges and Universities. A.M.D. is supported by the SNSF project “The Non-Gaussian Universe and Cosmological Symmetries”, project number:200020-178787. A.M.D. also acknowledges partial support from Tomalla Foundation for Gravity. We acknowledge the use of following packages in this work: Astropy [102, 103], Giant-Triangle-Confusogram [104], IPython [105], Matplotlib [106], NumPy [107], and SciPy [108]. The authors would like to thank the LIGO/Virgo scientific collaboration for providing the noise curves. LIGO is funded by the U.S. National Science Foundation. Virgo is funded by the French Centre National de Recherche Scientifique (CNRS), the Italian Istituto Nazionale della Fisica Nucleare (INFN), and the Dutch Nikhef, with contributions by Polish and Hungarian institutes. This material is based upon work supported by NSF’s LIGO Laboratory which is a major facility fully funded by the National Science Foundation.

* smukherjee1@perimeterinstitute.ca

† Azadeh.MoradinezhadDizgah@unige.ch

- [1] J. Aasi et al. (LIGO Scientific), *Class. Quant. Grav.* **32**, 074001 (2015), 1411.4547.
- [2] B. P. Abbott et al., *Phys. Rev. D* **93**, 112004 (2016), [Addendum: *Phys.Rev.D* 97, 059901 (2018)], 1604.00439.
- [3] F. Acernese, M. Agathos, K. Agatsuma, D. Aisa, N. Allemandou, A. Allocca, J. Amarni, P. Astone, G. Balestri, G. Ballardin, et al., *Classical and Quantum Gravity* **32**, 024001 (2014), ISSN 1361-6382, .
- [4] F. Acernese, M. Agathos, L. Aiello, A. Allocca, A. Amato, S. Ansoldi, S. Antier, M. Arène, N. Arnaud, S. Ascenzi, et al. (Virgo Collaboration), *Phys. Rev. Lett.* **123**, 231108 (2019), .
- [5] B. P. Abbott et al. (KAGRA, LIGO Scientific, VIRGO), *Living Rev. Rel.* **21**, 3 (2018), 1304.0670.
- [6] T. Akutsu et al. (KAGRA), *Nat. Astron.* **3**, 35 (2019), 1811.08079.
- [7] T. Akutsu et al. (KAGRA), arXiv:2005.05574 (2020), 2005.05574.
- [8] B. P. Abbott, R. Abbott, T. D. Abbott, M. R. Abernathy, F. Acernese, K. Ackley, C. Adams, T. Adams, P. Addesso, R. X. Adhikari, et al. (LIGO Scientific Collaboration and Virgo Collaboration), *Phys. Rev. Lett.* **116**, 061102 (2016), .
- [9] B. P. Abbott et al. (LIGO Scientific, Virgo), *Phys. Rev. Lett.* **119**, 161101 (2017), 1710.05832.
- [10] B. Abbott et al. (LIGO Scientific, Virgo), *Astrophys. J. Lett.* **882**, L24 (2019), 1811.12940.
- [11] R. Abbott et al. (LIGO Scientific, Virgo), *Astrophys. J. Lett.* **913**, L7 (2021), 2010.14533.
- [12] B. Abbott, R. Abbott, T. Abbott, S. Abraham, F. Acernese, K. Ackley, C. Adams, R. Adhikari, V. Adya, C. Affeldt, et al., *Physical Review X* **9** (2019), ISSN 2160-3308, .
- [13] R. Abbott, T. Abbott, S. Abraham, F. Acernese, K. Ackley, A. Adams, C. Adams, R. Adhikari, V. Adya, C. Affeldt, et al., *Physical Review X* **11** (2021), ISSN 2160-3308, .
- [14] R. Abbott et al. (LIGO Scientific, VIRGO, KAGRA Scientific) (2021), 2111.03634.
- [15] R. Abbott et al. (LIGO Scientific, VIRGO, KAGRA) (2021), 2111.03606.
- [16] Virgo and Kagra (LIGO Scientific, VIRGO, KAGRA) (2021), 2111.03604.
- [17] M. Fishbach, D. E. Holz, and W. M. Farr, *Astrophys. J. Lett.* **863**, L41 (2018), 1805.10270.
- [18] M. C. Artale, M. Mapelli, N. Giacobbo, N. B. Sabha, M. Spera, F. Santoliquido, and A. Bressan, *Mon. Not. Roy. Astron. Soc.* **487**, 1675 (2019), 1903.00083.
- [19] M. C. Artale, M. Mapelli, Y. Bouffanais, N. Giacobbo, M. Spera, and M. Pasquato, *Mon. Not. Roy. Astron. Soc.* **491**, 3419 (2020), 1910.04890.
- [20] F. Santoliquido, M. Mapelli, Y. Bouffanais, N. Giacobbo, U. N. Di Carlo, S. Rastello, M. C. Artale, and A. Ballone, *Astrophys. J.* **898**, 152 (2020), 2004.09533.
- [21] E. D. Kovetz et al. (2017), 1709.09066.
- [22] O. Doré et al. (SPHEREX) (2014), 1412.4872.
- [23] A. Aghamousa et al. (DESI) (2016), 1611.00036.
- [24] C. C. Diaz and S. Mukherjee, arXiv:2107.12787 (2021), 2107.12787.
- [25] S. Mukherjee, B. D. Wandelt, S. M. Nissanke, and A. Silvestri, *Phys. Rev. D* **103**, 043520 (2021), 2007.02943.
- [26] G. Scelfo, M. Spinelli, A. Raccanelli, L. Boco, A. Lapi, and M. Viel (2021), 2106.09786.
- [27] R. O’Shaughnessy, V. Kalogera, and K. Belczynski, *ApJ* **716**, 615 (2010), 0908.3635.
- [28] S. Banerjee, H. Baumgardt, and P. Kroupa, *MNRAS* **402**, 371 (2010), 0910.3954.
- [29] M. Dominik, K. Belczynski, C. Fryer, D. E. Holz, E. Berti, T. Bulik, I. Mandel, and R. O’Shaughnessy, *ApJ* **759**, 52 (2012), 1202.4901.
- [30] M. Dominik, E. Berti, R. O’Shaughnessy, I. Mandel, K. Belczynski, C. Fryer, D. E. Holz, T. Bulik, and F. Pannarale, *Astrophys. J.* **806**, 263 (2015), 1405.7016.
- [31] I. Mandel and S. E. de Mink, *MNRAS* **458**, 2634 (2016), 1601.00007.
- [32] A. Lamberts, S. Garrison-Kimmel, D. R. Clausen, and P. F. Hopkins, *Mon. Not. Roy. Astron. Soc.* **463**, L31 (2016), 1605.08783.
- [33] L. Cao, Y. Lu, and Y. Zhao, *MNRAS* **474**, 4997 (2018), 1711.09190.
- [34] O. D. Elbert, J. S. Bullock, and M. Kaplinghat, *Mon.*

- Not. Roy. Astron. Soc. **473**, 1186 (2018), 1703.02551.
- [35] J. J. Eldridge, E. R. Stanway, and P. N. Tang, *Mon. Not. Roy. Astron. Soc.* **482**, 870 (2019), 1807.07659.
- [36] L. du Buisson, P. Marchant, P. Podsiadlowski, C. Kobayashi, F. B. Abdalla, P. Taylor, I. Mandel, S. E. de Mink, T. J. Moriya, and N. Langer, *Mon. Not. Roy. Astron. Soc.* **499**, 5941 (2020), 2002.11630.
- [37] F. Santoliquido, M. Mapelli, N. Giacobbo, Y. Bouffanais, and M. C. Artale, *Mon. Not. Roy. Astron. Soc.* **502**, 4877 (2021), 2009.03911.
- [38] K. S. McCarthy, Z. Zheng, and E. Ramirez-Ruiz, *Mon. Not. Roy. Astron. Soc.* **499**, 5220 (2020), 2007.15024.
- [39] M. Toffano, M. Mapelli, N. Giacobbo, M. C. Artale, and G. Ghirlanda, *Mon. Not. Roy. Astron. Soc.* **489**, 4622 (2019), 1906.01072.
- [40] M. Fishbach and V. Kalogera, *Astrophys. J. Lett.* **914**, L30 (2021), 2105.06491.
- [41] S. Mukherjee and J. Silk, arXiv:2105.11139 (2021), 2105.11139.
- [42] P. Madau and M. Dickinson, *Annual Review of Astronomy and Astrophysics* **52**, 415–486 (2014), ISSN 1545-4282, .
- [43] P. S. Behroozi, R. H. Wechsler, and C. Conroy, *Astrophys. J.* **762**, L31 (2013), 1209.3013.
- [44] M. Safarzadeh and E. Berger, *ApJL* **878**, L12 (2019), 1904.08436.
- [45] M. Safarzadeh, E. Berger, J. Leja, and J. S. Speagle, *ApJL* **878**, L14 (2019), 1905.04310.
- [46] S. Adhikari, M. Fishbach, D. E. Holz, R. H. Wechsler, and Z. Fang, *ApJ* **905**, 21 (2020), 2001.01025.
- [47] M. Oguri, *Phys. Rev. D* **93**, 083511 (2016), .
- [48] S. Mukherjee and B. D. Wandelt, arXiv:1808.06615 (2018), 1808.06615.
- [49] S. Mukherjee, B. D. Wandelt, and J. Silk, *Phys. Rev. D* **101**, 103509 (2020), 1908.08950.
- [50] S. Mukherjee, B. D. Wandelt, and J. Silk, *Mon. Not. Roy. Astron. Soc.* **494**, 1956 (2020), 1908.08951.
- [51] F. Calore, A. Cuoco, T. Regimbau, S. Sachdev, and P. D. Serpico, *Physical Review Research* **2** (2020), ISSN 2643-1564, .
- [52] G. Scelfo, L. Boco, A. Lapi, and M. Viel, *JCAP* **10**, 045 (2020), 2007.08534.
- [53] S. Bera, D. Rana, S. More, and S. Bose, *Astrophys. J.* **902**, 79 (2020), 2007.04271.
- [54] S. Mukherjee, B. D. Wandelt, and J. Silk, *Mon. Not. Roy. Astron. Soc.* **502**, 1136 (2021), 2012.15316.
- [55] G. Cañas-Herrera, O. Contigiani, and V. Vardanyan, *ApJ* **918**, 20 (2021), 2105.04262.
- [56] G. Favole et al., *Mon. Not. Roy. Astron. Soc.* **497**, 5432 (2020), 1908.05626.
- [57] S. Yang and A. Lidz, *Monthly Notices of the Royal Astronomical Society* **499**, 3417–3433 (2020), ISSN 1365-2966, .
- [58] L. J. Kewley, M. J. Geller, and R. A. Jansen, *Astron. J.* **127**, 2002 (2004), astro-ph/0401172.
- [59] G. Lagache, M. Cousin, and M. Chatzikos, *A&A* **609**, A130 (2018), 1711.00798.
- [60] G. Sun, B. S. Hensley, T.-C. Chang, O. Doré, and P. Serra, *The Astrophysical Journal* **887**, 142 (2019), ISSN 1538-4357, .
- [61] R. Kannan, A. Smith, E. Garaldi, X. Shen, M. Vogelsberger, R. Pakmor, V. Springel, and L. Hernquist (2021), 2111.02411.
- [62] R. C. Kennicutt, Jr., *Ann. Rev. Astron. Astrophys.* **36**, 189 (1998), astro-ph/9807187.
- [63] C. Ly, M. A. Malkan, N. Kashikawa, K. Shimasaku, M. Doi, T. Nagao, M. Iye, T. Kodama, T. Morokuma, and K. Motohara, *Astrophys. J.* **657**, 738 (2007), astro-ph/0610846.
- [64] M. B. Silva, M. G. Santos, A. Cooray, and Y. Gong, *Astrophys. J.* **806**, 209 (2015), 1410.4808.
- [65] J. Kamenetzky, N. Rangwala, J. Glenn, P. R. Maloney, and A. Conley, *The Astrophysical Journal* **829**, 93 (2016), ISSN 1538-4357, .
- [66] Y. Gong, A. Cooray, M. B. Silva, M. Zemcov, C. Feng, M. G. Santos, O. Dore, and X. Chen, *The Astrophysical Journal* **835**, 273 (2017), ISSN 1538-4357, .
- [67] T. Y. Li, R. H. Wechsler, K. Devaraj, and S. E. Church, *Astrophys. J.* **817**, 169 (2016), 1503.08833.
- [68] J. Comparat et al., *Mon. Not. Roy. Astron. Soc.* **461**, 1076 (2016), 1605.02875.
- [69] S. Saito, S. de la Torre, O. Ilbert, C. Dubois, K. Yabe, and J. Coupon, *Mon. Not. Roy. Astron. Soc.* **494**, 199 (2020), 2003.06394.
- [70] N. Kaiser, *Mon. Not. Roy. Astron. Soc.* **227**, 1 (1987).
- [71] J. C. Jackson, *Mon. Not. Roy. Astron. Soc.* **156**, 1P (1972), 0810.3908.
- [72] C. Alcock and B. Paczynski, *Nature* **281**, 358 (1979).
- [73] A. Lidz and J. Taylor, *Astrophys. J.* **825**, 143 (2016), 1604.05737.
- [74] Y.-T. Cheng, T.-C. Chang, J. Bock, C. M. Bradford, and A. Cooray, *Astrophys. J.* **832**, 165 (2016), 1604.07833.
- [75] Y. Gong, X. Chen, and A. Cooray, *Astrophys. J.* **894**, 152 (2020), 2001.10792.
- [76] A. Moradinezhad Dizgah, G. K. Keating, K. S. Karkare, A. Crites, and S. R. Choudhury (2021), 2110.00014.
- [77] E. D. Hall and M. Evans, *Classical and Quantum Gravity* **36**, 225002 (2019), 1902.09485.
- [78] M. Maggiore et al., *JCAP* **03**, 050 (2020), 1912.02622.
- [79] P. Amaro-Seoane, H. Audley, S. Babak, J. Baker, E. Barausse, P. Bender, E. Berti, P. Binetruy, M. Born, D. Bortoluzzi, et al., arXiv e-prints arXiv:1702.00786 (2017), 1702.00786.
- [80] N. Aghanim et al. (Planck), arXiv: 1807.06209 (2018), 1807.06209.
- [81] B. Farr et al., *Astrophys. J.* **825**, 116 (2016), 1508.05336.
- [82] S. Mastrogiovanni, K. Leyde, C. Karathanasis, E. Chassande-Mottin, D. A. Steer, J. Gair, A. Ghosh, R. Gray, S. Mukherjee, and S. Rinaldi, *Phys.Rev.D* **104**, 062009 (2021), 2103.14663.
- [83] E. Schaan and M. White, *JCAP* **05**, 067 (2021), 2103.01971.
- [84] Y. B. Zel’dovich and I. D. Novikov, *Soviet Astronomy* **10**, 602 (1967).
- [85] S. Hawking, *MNRAS* **152**, 75 (1971).
- [86] B. J. Carr, *ApJ* **201**, 1 (1975).
- [87] M. Y. Khlopov and A. G. Polnarev, *Physics Letters B* **97**, 383 (1980).
- [88] M. I. Khlopov, B. A. Malomed, and I. B. Zeldovich, *MNRAS* **215**, 575 (1985).
- [89] B. J. Carr, in *59th Yamada Conference on Inflating Horizon of Particle Astrophysics and Cosmology* (2005), astro-ph/0511743.
- [90] S. Bird, I. Cholis, J. B. Muñoz, Y. Ali-Haïmoud, M. Kamionkowski, E. D. Kovetz, A. Raccanelli, and A. G. Riess, *Phys. Rev. Lett.* **116**, 201301 (2016),

- 1603.00464.
- [91] S. Clesse and J. García-Bellido, *Phys. Dark Univ.* **15**, 142 (2017), 1603.05234.
- [92] M. Sasaki, T. Suyama, T. Tanaka, and S. Yokoyama, *Phys. Rev. Lett.* **117**, 061101 (2016), [Erratum: *Phys.Rev.Lett.* 121, 059901 (2018)], 1603.08338.
- [93] M. Raidal, V. Vaskonen, and H. Veermäe, *JCAP* **09**, 037 (2017), 1707.01480.
- [94] M. Raidal, C. Spethmann, V. Vaskonen, and H. Veermäe, *JCAP* **02**, 018 (2019), 1812.01930.
- [95] A. D. Gow, C. T. Byrnes, A. Hall, and J. A. Peacock, *JCAP* **01**, 031 (2020), 1911.12685.
- [96] K. Jedamzik, *JCAP* **09**, 022 (2020), 2006.11172.
- [97] K. Jedamzik, *Phys. Rev. Lett.* **126**, 051302 (2021), 2007.03565.
- [98] V. De Luca, G. Franciolini, P. Pani, and A. Riotto, *JCAP* **06**, 044 (2020), 2005.05641.
- [99] V. Vaskonen and H. Veermäe, *Phys. Rev. D* **101**, 043015 (2020), 1908.09752.
- [100] V. Atal, A. Sanglas, and N. Triantafyllou, *JCAP* **11**, 036 (2020), 2007.07212.
- [101] S. Mukherjee, M. S. P. Meinema, and J. Silk (2021), 2107.02181.
- [102] Astropy Collaboration, T. P. Robitaille, E. J. Tollerud, P. Greenfield, M. Droettboom, E. Bray, T. Aldcroft, M. Davis, A. Ginsburg, A. M. Price-Whelan, et al., *A&A* **558**, A33 (2013), 1307.6212.
- [103] Astropy Collaboration, A. M. Price-Whelan, B. M. Sipőcz, H. M. Günther, P. L. Lim, S. M. Crawford, S. Conseil, D. L. Shupe, M. W. Craig, N. Dencheva, et al., *AJ* **156**, 123 (2018), 1801.02634.
- [104] S. Bocquet and F. W. Carter, *The Journal of Open Source Software* **1** (2016), .
- [105] F. Pérez and B. E. Granger, *Computing in Science and Engineering* **9**, 21 (2007), ISSN 1521-9615, .
- [106] J. D. Hunter, *Computing In Science & Engineering* **9**, 90 (2007).
- [107] S. van der Walt, S. C. Colbert, and G. Varoquaux, *Computing in Science and Engineering* **13**, 22 (2011), 1102.1523.
- [108] E. Jones, T. Oliphant, P. Peterson, et al., *SciPy: Open source scientific tools for Python* (2001–), [Online; accessed ;today;], .